Formulation of a mixed-mode multilinear cohesive zone law in an interface finite element for modelling delamination with R-curve effects

Mosbjerg Jensen, Simon; Martos, M. J.; Bak, Brian Lau Verndal; Lindgaard, Esben

Published in:
Composite Structures

DOI (link to publication from Publisher):
10.1016/j.compstruct.2019.02.029

Publication date:
2019

Document Version
Accepted author manuscript, peer reviewed version

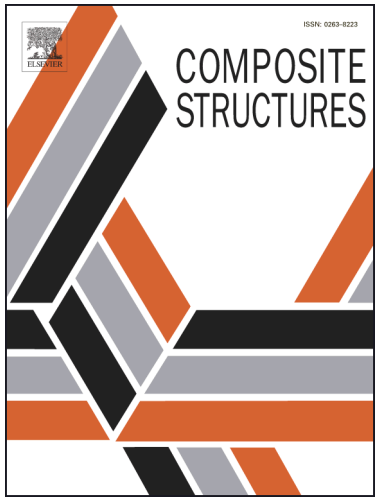

Formulation of a Mixed-mode Multilinear Cohesive Zone Law in an Interface Finite Element for Modelling Delamination with R-curve Effects

S.M. Jensen, M.J. Martos, B.L.V. Bak, E. Lindgaard

PII: S0263-8223(18)33738-3
DOI: https://doi.org/10.1016/j.compstruct.2019.02.029
Reference: COST 10654

To appear in: *Composite Structures*

Received Date: 15 October 2018
Revised Date: 22 December 2018
Accepted Date: 8 February 2019

Please cite this article as: Jensen, S.M., Martos, M.J., Bak, B.L.V., Lindgaard, E., Formulation of a Mixed-mode Multilinear Cohesive Zone Law in an Interface Finite Element for Modelling Delamination with R-curve Effects, *Composite Structures* (2019), doi: https://doi.org/10.1016/j.compstruct.2019.02.029

Formulation of a Mixed-mode Multilinear Cohesive Zone Law in an Interface Finite Element for Modelling Delamination with R-curve Effects

S.M. Jensen[a,*], M.J. Martos[a], B.L.V. Bak[a], E. Lindgaard[a]

[a]*Department of Materials and Production, Aalborg University, Fibigerstræde 16, Aalborg DK-9220, Denmark*

Abstract

A constitutive model for an interface finite element is proposed to enable simulation of delamination in composite materials with R-curve effects. The constitutive model is formulated in the framework of cohesive zone modelling (CZM). In essence, a multilinear CZ law with an arbitrary number of line segments is developed. The CZ law seeks to enable constitutive modelling of failure mechanisms on multiple scales within the fracture process zone and reduce conventional a priori assumptions regarding the shape of the CZ law. The CZ law relies on damage mechanics, an equivalent one-dimensional formulation, and criteria for mode interactions to simulate delamination under mixed-mode loading. Special emphasis is put on the derivation of interpolation formulas and a constitutive tangent stiffness tensor for the multilinear formulation. The constitutive model is implemented in the commercial FE program ANSYS Mechanical, for implicit finite element analysis (FEA), using user-programmable features. The implementation is verified through single interface element numerical studies, and its applicability is demonstrated by simulating an experiment of quasi-static delamination showing large-scale fiber bridging in pure mode I DCB glass-fiber epoxy specimens. Experimental measurements and simulation outputs using the novel cohesive element is compared to those of the conventional bi- and trilinear CZ laws.

Keywords: Delamination, cohesive zone model, interface finite element, damage modelling, mixed-mode fracture, fiber bridging

1. Introduction

A commonly occurring failure type in engineering composite structures is delamination due to the relatively weak interface strength of a laminate. Delamination can be caused by numerous reasons, e.g. high peel stresses near free edges of a laminate, stress concentrations due to structural joints, or manufacturing defects. Assessment of delamination initiation and propagation is crucial to the design engineer for damage tolerance prediction of general engineering structures, and brings knowledge of failure mechanisms occurring in the fracture process, which also proves valuable in the field of microstructural optimization and development of new materials. A commonly utilized approach for assessment of delamination in composites is using cohesive zone modelling (CZM) in combination with the finite element method (FEM). CZM was initiated in the late 50'ties and the early 60'ties by Barenblatt [1] and Dugdale [2]. They developed similar mathematical models from different physical perspectives resulting in finite stresses at the crack tip, and thereby avoiding non-physical singular stresses as known from linear elastic fracture mechanics (LEFM). During the following two decades advances in CZM impelled a specially attractive framework for FEA of interfacial debonding and delamination analyses having the capability of modelling both crack initiation and propagation [3, 4]. Further development has lead to state-of-the-art approaches for FEA of delamination using CZM in an interface element formulation, see e.g. [5–8].

The fundamental idea of CZM is that the resistance to crack initiation and propagation can be represented by a distribution of tractions acting on separated crack faces in a cohesive zone at/near the crack tip. Interfacial tractions τ_i are related to interfacial separations Δ_j of the crack faces through CZ laws.

*Corresponding author E-mail address: smj@m-tech.aau.dk

The CZ laws are interfacial constitutive laws defined point-wise within the cohesive zone and relate tractions to separations of initially coinciding points of the crack faces. The interfacial constitutive behaviour articulates in the shape of the CZ law. Various shapes of CZ laws have been proposed in the open literature of CZM and applied for simulation of crack initiation and growth. Hillerborg [3] and Needleman [4] used a bilinear and a polynomial traction-separation relation, respectively. In the work of Tvergaard and Hutchinson [9] the fracture toughness of ductile adhesive joints are studied using a trapezoidal CZ law. Goyal et al. [10] formulated an exponential CZ law, while Camamho et al. [5] and Turon [11] used a bilinear CZ law, the latter for use in fatigue loading of laminated composites. A benchmark study and comparison of prevalent CZ laws is performed by Alfano [12], wherein it is concluded, that the specific shape of the CZ law has little influence on the crack propagation characteristics. However, the insignificance of the shape of the CZ law is only true for conditions of small-scale fracture process zones, that is, the size of the fracture process zone is small compared with the crack length and the remaining physical dimensions of the specimen under consideration.

Large-scale fracture process zones involve multiple failure mechanisms occurring at different length scales. In fiber reinforced composites the near-crack tip failure mechanisms are typically governed by matrix micro-cracking and plastic/viscoelastic deformation along with void nucleation, -growth and -coalescence. Fiber bridging occurs in the wake of the crack tip, which cause increasing fracture resistance as the crack evolves i.e. R-curve behaviour. In such material systems, e.g. glass fiber-epoxy composites, the shape of the CZ law becomes important for crack propagation characteristics [7, 13].

In the open literature, there is a difference in opinion, whether the CZ law is an inherent property of the constituent materials or if it also depends on the specimen geometry in presence of large-scale fiber bridging. In particular, the dependence of specimen thickness has been subject to investigation. Sørensen et al. [13] studied UD carbon-epoxy DCB specimens subjected to pure bending, and measured R-curves for specimens of various thickness. The CZ law proved to be independent of the specimen thickness as the R-curves, in terms of energy release rate versus end-opening displacement, are coincident. However, in a similar experimental campaign of UD carbon-epoxy DCB specimens performed by Farmand et al. [14], the CZ law is shown to depend on the specimen thickness. In specific, the results prove that the plateau level of the energy release rate, graphed versus the crack extent, increases with specimen thickness. Canal et al. [15] supports the opinion that bridging tractions depend on specimen geometry. In their work, thickness scaling effects are addressed by augmenting the CZ law, formulated as a traction-separation relation, with information of local angles of rotation and bridging tractions extracted from micro-mechanical simulations. Accordingly, there is no clear consensus whether the CZ law can be considered a material property or not.

Nevertheless in order to simulate delamination in material systems with large-scale fiber bridging, one requires a constitutive model that can represent failure mechanisms on both small and large scales. This can be accomplished by adding complexity to the shape of the CZ law. Sorensen et al. [16] used a two-part traction-separation relation to simulate mode I delamination in CFRP composites with large scale fiber bridging. The first part of the CZ law is taken to be a bilinear traction-separation relation, which accounts for crack initiation, while the second part of the CZ law describes the bridging traction distribution with an exponential decaying function. Hansen et al. [7] proposed a CZ model for simulating multi-scale fracture mechanisms in glass-epoxy laminates using a combination of bilinear and higher-order polynomial functions. Other attempts have been proposed in the work [17–19] using trilinear CZ laws, wherein one line segment is added to the conventional bilinear CZ law to provide a simple linear representation of the bridging traction distribution.

In the present work the CZ law is treated as an inherent material property. The CZ law is formulated in the constitutive model of an interface finite element, as a mixed-mode multilinear traction-separation relation with an arbitrary number of line segments. The work takes point of departure in the CZM proposed in [20], which relies on a mixed-mode bilinear CZ law. The multilinear formulation is motivated by the insufficiency of the bilinear formulation to simulate crack propagation when R-curve behaviour is prominent. The shortcomings of the bilinear formulation for modelling R-curve effects is illustrated by applying it to simulate delamination in a real experiment using UD glass fiber-epoxy laminated DCB specimens. Additionally, a trilinear CZ law is tested to simulate the same experiment, and its limited capability to simulate the experimental response provides further physical reasoning and motivation for adding complexity to the traction-separation relation. The multilinear formulation works with an arbitrary number of line segments, but it is tested here using a 15-segmented CZ law. The simulation shows excellent agreement with the experiment.

The structure of the paper is as follows. Section 2 describes the essentials of the cohesive zone model with special focus on constitutive relations, damage formulation, mode interactions, and the constitutive tangent stiffness tensor. The topics of section 3 are the numerical implementation and verification studies of the user-programmed cohesive interface element. Lastly, section 4 demonstrates the applicability of the multilinear CZ law by simulating quasi-static delamination in UD glass fiber-epoxy specimens with R-curve effects.

2. Cohesive Zone Model

The mechanics of CZM require a kinematic model and a constitutive model for a complete description, however, this paper is concerned with the latter. The current FE implementation takes point of departure in the CZM proposed in [20], and no changes will be done to the kinematic description. However, for completeness and ease of reading, a brief summary of the kinematic model in [20] is given first.

2.1. Interface Kinemtics

The interfacial kinematics is defined according to a midsurface $\bar{S}$, to which the delamination path is assumed to be coincident. The interfacial surface is an interior surface of discontinuity in displacements, and is illustrated in Fig. 1 during a deformation process. Surfaces S^+ and S^- represent the upper and lower crack face, respectively. In the undeformed configuration, the surfaces S^+, S^-, $\bar{S}$ are coincident with a reference surface S^0. In the deformed configuration, the midsurface is formed by the set of points $\bar{P}$, which is the average distance between points P^+ and P^- contained in S^+ and S^-, respectively. Coordinates of the midsurface $\bar{x}_i$ in terms of the global Cartesian coordinate system is written in Eq. (1):

$$\bar{x}_i = X_i^0 + \frac{1}{2}\left(u_i^+ + u_i^-\right) \tag{1}$$

Where X_i^0 are the global Cartesian coordinates of an arbitrary point in the undeformed configuration, e.g. P^0, and $u_i^{\pm}$ describes the displacement of the point measured along the global Cartesian coordinate system X_i.

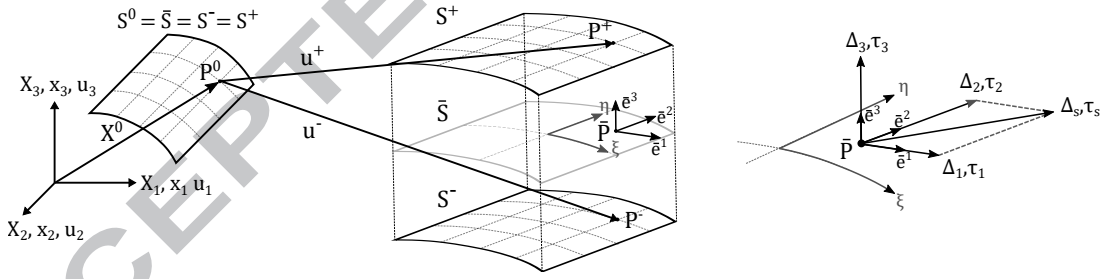

Figure 1: Interfacial surfaces in undeformed and deformed configurations. The concept of a mid-surface $\bar{S}$ from which the interfacial mechanics of the CZM is defined. $(\bar{e}^1, \bar{e}^2, \bar{e}^3)$ is a local Cartesian coordinate system defined at the deformed midsurface.

The constitutive relations of the CZM are defined in terms of local interfacial tractions τ_i and separations Δ_j. These are described according to a local coordinate system $(\bar{e}^1, \bar{e}^2, \bar{e}^3)$ which expresses normal directions $\bar{e}^3$ and tangential directions $\bar{e}^1, \bar{e}^2$ at some point at the deformed midsurface. The local coordinate system is constructed from a curvilinear coordinate system $(\xi,\ \eta)$ located on the midsurface. Tangential directions are obtained as the curvilinear gradients of the midsurface, denoted by $v_i^{\xi} = \bar{x}_{i,\xi}$ and $v_i^{\eta} = \bar{x}_{i,\eta}$. In general, the curvilinear coordinates, and hence the gradients v_i^{ξ} and v_i^{η}, are not mutually orthogonal. Consequently, the local orthonormal coordinate system $(\bar{e}^1, \bar{e}^2, \bar{e}^3)$ is established using cross products and norms of the tangential curvilinear gradients.

$$\bar{e}_i^1 = \frac{v_i^{\xi}}{|v_i^{\xi}|}, \qquad \bar{e}_i^3 = \frac{v_i^{\xi} \times v_i^{\eta}}{|v_i^{\xi} \times v_i^{\eta}|}, \qquad \bar{e}_i^2 = \bar{e}_i^3 \times \bar{e}_i^1, \qquad \Theta_{ij} = \begin{bmatrix} \bar{e}_1^1 & \bar{e}_2^1 & \bar{e}_3^1 \\ \bar{e}_1^2 & \bar{e}_2^2 & \bar{e}_3^2 \\ \bar{e}_1^3 & \bar{e}_2^3 & \bar{e}_3^3 \end{bmatrix} \tag{2}$$

The components of $(\bar{e}_i^1, \bar{e}_i^2, \bar{e}_i^3)$ defines a transformation tensor Θ_{ij} between the global Cartesian coordinate system (X_1, X_2, X_3) and the local coordinate system $(\bar{e}^1, \bar{e}^2, \bar{e}^3)$. Local normal and local tangential interfacial separations can then be expressed in terms of the transformation tensor Θ_{ij} and the global displacement vectors $u_i^{\pm}$.

$$\Delta_i = \Theta_{ij}\left(u_j^+ - u_j^-\right) \tag{3}$$

It is noted, that the transformation is formulated without reference to the crack front orientation in the specimen. Consequently, the kinematic interface model is incapable of distinguishing between crack opening modes associated with the tangential directions i.e. mode II and mode III. Therefore, a combined shear mode s is introduced, which is spanned by the local tangential directions $\bar{e}_i^1$ and $\bar{e}_i^2$ as illustrated in Fig. 1. However, the recent work in [21] on evaluation of the crack growth driving direction in three-dimensional structures from pure local element information, may provide a future means of distinguishing between the shear modes.

2.2. Constitutive Relations

A secant constitutive equation, which computes interfacial tractions for any value of the interfacial separations Δ_j and damage variable d, is derived from a free energy potential in Turon et al. [22] and is repeated in Eq. (4). Herein D_{ij}^0 is a second order stiffness tensor of the pristine material interface, which corresponds to the penalty stiffness K. In case of equal penalty stiffness $K^{(eq)}$ in the three basic directions, the undamaged stiffness tensor reduces to $D_{ij}^0 = K^{(eq)}\delta_{ij}$, with δ_{ij} being Kronecker's delta. As damage evolves, the effective interfacial stiffness $(1-d)D_{ij}^0$ decreases.

$$\tau_i = (1-d)D_{ij}^0\Delta_j - dD_{ij}^0\delta_{3j}\langle-\Delta_3\rangle \tag{4}$$

Any negative value of the local separation component Δ_3, which is associated with mode I crack opening is non-physical as interpenetration is prevented by contact. The Macaulay bracket, $\langle x\rangle = \frac{1}{2}(x + |x|)$, in the second term of Eq. (4), ensures that the stiffness is unaffected by damage and becomes equal to the penalty stiffness in case of negative Δ_3.

2.3. Damage Model

The damage model describes the evolution of a damage variable d, which controls the degradation of the interfacial stiffness during the crack process. The damage variable develops concurrently with the fracture energy dissipation, and should be a monotonically increasing scalar to ensure irreversibility. For a pristine interface, the damage variable equals zero $d = 0$. Upon full damage it equals unity $d = 1$, in which case, the effective interfacial stiffness $K^{(eq)}(1-d)$ and the interfacial tractions are zero.

The damage variable evolves according to an equivalent one-dimensional CZ law and a damage criterion. The equivalent one-dimensional CZ law, Eq. (5), relates a work conjugate traction norm $\bar{\sigma}$ and the equivalent separation norm λ [22], as a function of the damage variable d and the penalty stiffness $K^{(eq)}$. The $(\bar{\sigma}, \lambda)$-relation is piecewise linear in shape with an arbitrary number of line segments, and is referred to in the following as the equivalent one-dimensional multilinear CZ law.

$$\bar{\sigma} = K^{(eq)}(1-d)\lambda \qquad \lambda = \sqrt{\Delta_s^2 + \langle\Delta_3\rangle^2} \quad \text{for} \quad \Delta_s = \sqrt{\Delta_1^2 + \Delta_2^2} \tag{5}$$

2.3.1. Mode Interaction

An equivalent one-dimensional multilinear CZ law is illustrated in Fig. 2. Let the CZ variables be values of tractions and separations at the end points of the line segments in the multilinear CZ law. The CZ variables will be denoted by $(\bar{\delta}^{(p-1)}, \bar{\sigma}^{(p-1)})$ and $(\bar{\delta}^{(p)}, \bar{\sigma}^{(p)})$, which represent the values of separations and tractions at the end points belonging to line segment p as illustrated in Fig. 2. Accordingly, a CZ law with n line segments is fully defined by $2n$ CZ variables.

The CZ variables $(\bar{\delta}^{(p)}, \bar{\sigma}^{(p)})$ are in general mode dependent. Mode interactions are taken into account by a set of interpolation formulas which evaluate equivalent one-dimensional CZ variables from pure mode CZ variables and some measure of the degree of mode-mixity. In the following, an overhead bar denotes equivalent one-dimensional

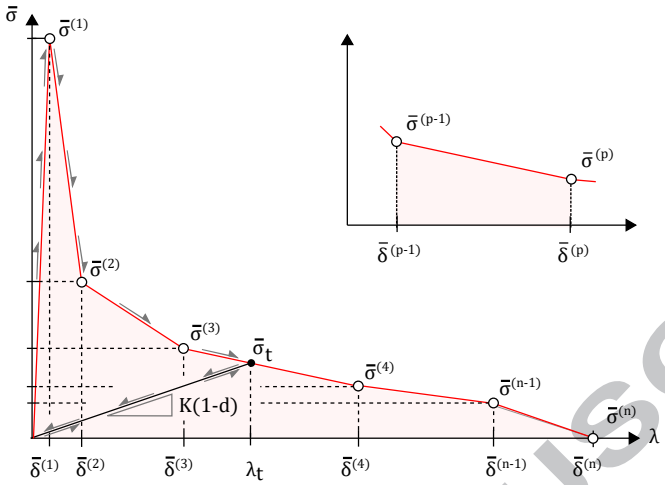

Figure 2: A mixed-mode multilinear CZ law. The equivalent traction-separation relation is piecewise defined, and every p'th line segment is defined by its end points $(\bar{\delta}^{(p-1)};\ \bar{\sigma}^{(p-1)})$ and $(\bar{\delta}^{(p)};\ \bar{\sigma}^{(p)})$. Note that the CZ law is shown for constant β.

properties, while sub-indices 3 and s refers to pure mode I and pure shear mode, respectively. The mode dependency of the traction variables $\bar{\sigma}^{(p)}$ will be taken into account using a strength criterion with quadratic stress interaction. The mode dependency of the separation variables $\bar{\delta}^{(p)}$ is derived from a crack propagation criterion, which yields a CZ law that is energy consistent with the modified BK-criterion [22, 23].

At first, a measure of the degree of mode-mixity is quantified. A β-parameter is introduced as an instantaneous and displacement-based measure of the local degree of mode-mixity, see Eq. (6) [22]. In a finite element framework, β is computed pointwise at every element integration point within the interface finite element from local interfacial separation components Δ_3 and Δ_s.

$$\beta = \frac{\Delta_s}{\Delta_s + \langle \Delta_3 \rangle} \tag{6}$$

Secondly, interpolation functions must be derived to determine the equivalent one-dimensional multilinear CZ law, as illustrated in Fig. 3: Given pure mode CZ variables and the degree of mode-mixity, how should the equivalent one-dimensional CZ law for mixed-mode loading be computed? The n-segmented multilinear CZ law contains $2n$ CZ variables: $\bar{\delta}^{(p)}$ and $\bar{\sigma}^{(p)}$ for $p = 1, \ldots, n$, and hence the same number of interpolation functions are required. The traction variables are interpolated using a strength criterion with quadratic stress interaction, see Eq. (7). The strength criterion was originally proposed in [22] as a mode dependent damage initiation criterion to interpolate the onset traction $\bar{\sigma}^{(1)}$ in a consistent way with the BK-criterion. Here the strength interaction criterion is adopted to every n traction variable $\bar{\sigma}^{(p)}$ of the multilinear CZ law.

$$(\bar{\sigma}^{(p)})^2 = (\sigma_3^{(p)})^2 + \left[(\sigma_s^{(p)})^2 - (\sigma_3^{(p)})^2\right] B^{\xi} \qquad \text{where} \qquad B = \frac{\beta^2}{1 + 2\beta^2 - 2\beta} \qquad \text{for} \quad p = 1, \ldots, n \tag{7}$$

Interpolation functions to compute the equivalent one-dimensional separation variables $\bar{\delta}^{(p)}$ will be derived from the modified BK-criterion. The original BK-criterion is a widely used crack propagation criterion and is reported to agree well with experimental data for epoxy resin composites [5, 23]. The modified BK-criterion computes the critical energy release rate G_c according to Eq. (8) [22], which implies that the mode II and III critical energy release rates are assumed to be equal $G_c^s = G_c^{II} = G_c^{III}$:

$$G_c = G_c^I + (G_c^s - G_c^I) B^{\eta} \tag{8}$$

Rice [24] showed using the J-integral, that the critical energy release rate is equal to the specific work done by interfacial tractions at the outermost point of the CZ when the crack is critically opened. Accordingly, the critical energy release rate G_c of the multilinear CZ law in Fig. 2 equals the shaded area under the $(\bar{\sigma},\ \lambda)$-curve.

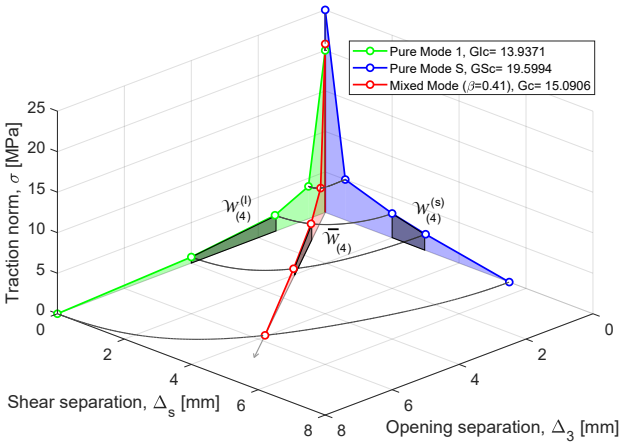

Figure 3: The equivalent one-dimensional CZ law (red) is interpolated from pure mode I (green) and mode S (blue) CZ laws for constant $\beta = 0.41$.

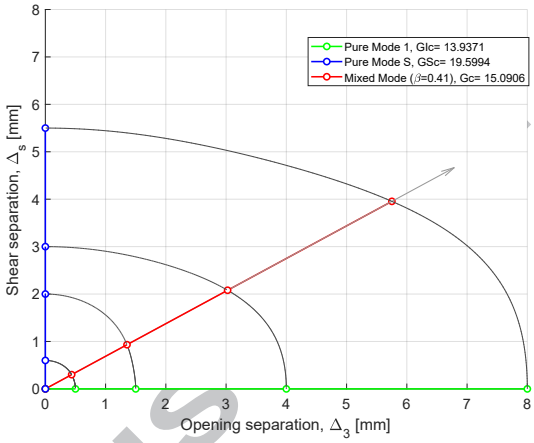

Figure 4: Interpolation of equivalent one-dimensional separation variables $\bar{\delta}^{(p)}$ for $p = 2, ..., 5$ according to Eq. (13).

This may be expressed as a sum of integrations for every two consecutive separation variables $\bar{\delta}^{(p-1)}$ and $\bar{\delta}^{(p)}$:

$$G_c = \int_0^{\bar{\delta}^{(n)}} \bar{\sigma}(\lambda) d\lambda = \sum_{p=1}^{n} \int_{\bar{\delta}^{(p-1)}}^{\bar{\delta}^{(p)}} \bar{\sigma}(\lambda) d\lambda = \sum_{p=1}^{n} \bar{\mathcal{W}}_{(p)} \tag{9}$$

Wherein $\bar{\delta}^{(0)} = 0$. The integral over the p'th interval $[\bar{\delta}^{(p-1)};\ \bar{\delta}^{(p)}]$ in Eq. (9), is related to the specific work performed by the interfacial tractions, and will be denoted by $\bar{\mathcal{W}}_{(p)}$. The notation is illustrated in Fig. 3 for the fourth line segment ($p = 4$). The area $\bar{\mathcal{W}}_{(4)}$ is composed of the CZ variables $\bar{\delta}^{(3)}, \bar{\delta}^{(4)}, \bar{\sigma}^{(4)}, \bar{\sigma}^{(3)}$. Applying this notation in the modified BK-criterion in Eq. (8), one obtain Eq. (10).

$$\sum_{p=1}^{n} \bar{\mathcal{W}}_{(p)} = \sum_{p=1}^{n} \left(\mathcal{W}^{I}_{(p)} + \left(\mathcal{W}^{s}_{(p)} - \mathcal{W}^{I}_{(p)} \right) B^{\eta} \right) \tag{10}$$

In order to arrive at a sufficient number of equations to determine every equivalent one-dimensional separation variable of the multilinear formulation, Eq. (10) is divided into n equations. This is done by applying the modified BK-interpolation function to sub-parts of the fracture energy $\bar{\mathcal{W}}$ rather than the total fracture energy $G_c = \sum \bar{\mathcal{W}}$, as shown in Eq. (11). A clarifying illustration of $\bar{\mathcal{W}}_{(p)}, \mathcal{W}^{I}_{(p)}$ and $\mathcal{W}^{s}_{(p)}$ are given in Fig. 3.

$$\bar{\mathcal{W}}_{(p)} = \mathcal{W}^{I}_{(p)} + \left(\mathcal{W}^{s}_{(p)} - \mathcal{W}^{I}_{(p)} \right) B^{\eta} \qquad \text{for} \quad p = 1, ..., n \tag{11}$$

Each integral $\bar{\mathcal{W}}_{(p)}$ can be computed exactly with a trapezoidal integration rule due to the piecewise linear formulation of the multilinear CZ law, see Eq. (12).

$$\bar{\mathcal{W}}_{(p)} = \frac{1}{2} \left(\bar{\sigma}^{(p)} + \bar{\sigma}^{(p-1)} \right) \left(\bar{\delta}^{(p)} - \bar{\delta}^{(p-1)} \right) \tag{12}$$

Combining Eq. (12) and Eq. (11), one obtains an equation for the p'th equivalent one-dimensional separation variable $\bar{\delta}^{(p)}$:

$$\bar{\delta}^{(p)} = \bar{\delta}^{(p-1)} + \frac{\mathcal{W}^{I}_{(p)} + \left(\mathcal{W}^{s}_{(p)} - \mathcal{W}^{I}_{(p)} \right) B^{\eta}}{\frac{1}{2} \left(\bar{\sigma}^{(p)} + \bar{\sigma}^{(p-1)} \right)} \qquad \text{for} \quad p = 2, ..., n \tag{13}$$

This equation applies for $p = 2, ..., n$. If $p = 1$ the separation variable is simply computed from the onset traction and the penalty stiffness: $\bar{\delta}^{(1)} = \bar{\sigma}^{(1)} / K^{(eq)}$. The interpolation of equivalent one-dimensional separation variables is illustrated in Fig. 4 by the black curves for $0 \leq \beta \leq 1$.

2.3.2. Damage Criterion

The irreversibility of the damage evolution process is taken into account by a damage criterion. The damage criterion is formulated such that the damage variable at the current pseudo solution time t is given according to Eq. (14).

$$d = \min(\max(0, \mathscr{D}_T), 1) \quad \forall \ T \in [0, t] \tag{14}$$

The evident cases of $d = 0$ and $d = 1$ corresponds to a pristine and fully damaged interface, respectively. An auxiliary damage function $\mathscr{D}$ is introduced. The auxiliary damage function derives from the intersection of the line of secant stiffness in Eq. (5) and the multilinear CZ law, as illustrated by the point $(\lambda_t, \bar{\sigma}_t)$ in Fig. 2, and describes the associated damage variables as λ varies. Effectively, $\mathscr{D}$ assumes that $(\bar{\sigma}_T, \ \lambda_T)$ at any time follows the multilinear CZ law.

The traction-separation relation of the multilinear CZ law is described by a set of linear Lagrange polynomials. Considering an arbitrary line segment p; a linear traction-separation relation can be expressed in terms the CZ variables associated with the current line segment: $(\bar{\delta}^{(p-1)};\ \bar{\sigma}^{(p-1)})$ and $(\bar{\delta}^{(p)};\ \bar{\sigma}^{(p)})$, as given in Eq. (15).

$$\bar{\sigma}(\lambda) = \frac{\bar{\sigma}^{(p)}\left(\lambda - \bar{\delta}^{(p-1)}\right) + \bar{\sigma}^{(p-1)}\left(\bar{\delta}^{(p)} - \lambda\right)}{\bar{\delta}^{(p)} - \bar{\delta}^{(p-1)}} \qquad \text{for} \quad \bar{\delta}^{(p-1)} \leq \lambda \leq \bar{\delta}^{(p)} \tag{15}$$

Combining Eq. (5) and Eq. (15) yields the auxiliary damage function in Eq. (16). This equation applies to the damage criterion in Eq. (14) to compute the current damage variable d. Note that the p-parameter must update according to the currently active line segment of the multilinear CZ law. This is ensured by appropriate bookkeeping in the numerical implementation.

$$\mathscr{D} = 1 + \frac{\bar{\sigma}^{(p)}(\bar{\delta}^{(p-1)} - \lambda) + \bar{\sigma}^{(p-1)}(\lambda - \bar{\delta}^{(p)})}{K^{(eq)}(\bar{\delta}^{(p)} - \bar{\delta}^{(p-1)})\lambda} \qquad \text{for} \quad \bar{\delta}^{(p-1)} \leq \lambda \leq \bar{\delta}^{(p)} \tag{16}$$

Crack propagation problems are inherently nonlinear and must be solved numerically using iterative solvers. In the finite element implementation, the damage criterion is formulated incrementally in displacement jump space. The damage criterion in Eq. (14) is hence reformulated in terms of a displacement-based damage threshold value r, as given in Eq. (17)-(18), which is equivalent to the original criterion. The superscript k refers to the current substep in the iterative solution procedure, while $k-1$ refers to the previously converged substep. The current damage threshold value r^k is the maximum value of the equivalent separation norm λ^k and the damage threshold value at the previous iteration r^{k-1}. The value of r^{k-1} is evaluated by rearranging terms in (16) to compute the equivalent separation norm $\lambda(d^{k-1})$ associated with the damage state in the previously converged substep. Note that the equivalent one-dimensional CZ variables, e.g. $\bar{\sigma}^{(p)}$ and $\bar{\delta}^{(p)}$, are dependent on the mode-mixity which makes the damage criterion applicable for varying crack opening mode.

$$r^k = \max(r^{k-1}, \lambda^k) \quad \text{where} \quad r^{k-1} = \frac{\bar{\sigma}^{(p-1)}\bar{\delta}^{(p)} - \bar{\sigma}^{(p)}\bar{\delta}^{(p-1)}}{\bar{\sigma}^{(p-1)} - \bar{\sigma}^{(p)} + K^{(eq)}(1 - d^{k-1})(\bar{\delta}^{(p)} - \delta^{(p-1)})} \tag{17}$$

$$d^k = \mathscr{D}^k\big|_{\lambda = r^k} \quad \text{for} \quad \bar{\delta}^{(1)} \leq \lambda \leq \bar{\delta}^{(n)} \tag{18}$$

2.4. Constitutive Tangent Stiffness Tensor

The rate of change of interfacial tractions is related to the rate of change of the interfacial separations by the constitutive tangent stiffness tensor as expressed in Eq. (19):

$$\frac{d\tau_i}{dt} = D_{ij}^{tan}\frac{d\Delta_j}{dt} \tag{19}$$

Where t represents a pseudo time during the iterative solution procedure. To establish an expression for the constitutive tangent stiffness tensor one needs the time derivative of Eq. (4). Recall that both the damage variable d and the interfacial separation Δ_j are functions of time.

$$\frac{d\tau_i}{dt} = -\dot{d}D_{ij}^0\Delta_j + (1-d)D_{ij}^0\dot{\Delta}_j - \dot{d}D_{ij}^0\delta_{3j}\langle-\Delta_3\rangle - dD_{ij}^0\delta_{3j}\frac{d(\langle-\Delta_3\rangle)}{dt} \tag{20}$$

The penalty stiffness are assumed to be constant in the three basic directions, such that the pristine stiffness tensor reads $D_{ij}^0 = \delta_{ij}K^{(eq)}$. Rearranging terms in Eq. (20), and utilizing that $d(\langle-\Delta_3\rangle)/dt = (\langle-\Delta_3\rangle/\Delta_3)\dot{\Delta}_3$, one arrives at Eq. (21). This equation is derived directly from the secant constitutive equation and is independent of the shape of the CZ law.

$$\dot{\tau}_i = \delta_{ij}K^{(eq)}\left[1 - d\left(1 + \delta_{3j}\frac{\langle-\Delta_3\rangle}{\Delta_3}\right)\right]\dot{\Delta}_j - \delta_{ij}K^{(eq)}\left[1 + \delta_{3j}\frac{\langle-\Delta_3\rangle}{\Delta_3}\right]\Delta_j\dot{d} \tag{21}$$

Since D_{ij}^{tan} explicitly relates $\dot{\tau}_i$ and $\dot{\Delta}_j$, an expression for the time derivative of the damage variable $\dot{d}$ is required. The damage variable depends on multiple intermediate variables: λ, $\bar{\sigma}^{(p-1)}, \bar{\sigma}^{(p)}, \bar{\delta}^{(p-1)}, \bar{\delta}^{(p)}$, see Eq. (14) and Eq. (16). These may vary with time and their time derivative should be computed according to Eq. (22). Following the argumentation in [22], the rate of change of the mode-mixity is sufficiently small to be negligible in real applications compared to the pseudo time increment taken in the iterative solution procedure. This argumentation implies that the time derivatives of the mode-dependent equivalent one-dimensional CZ variables become zero, e.g. $\dot{\bar{\sigma}}^{(p)} \approx 0$. Consequently, the time derivative of the damage variable simplifies according to the approximation in Eq. (22) and becomes proportional to the time derivative of the equivalent separation norm.

$$\dot{d} = \frac{\partial d}{\partial\lambda}\dot{\lambda} + \frac{\partial d}{\partial\bar{\sigma}^{(p-1)}}\dot{\bar{\sigma}}^{(p-1)} + \frac{\partial d}{\partial\bar{\sigma}^{(p)}}\dot{\bar{\sigma}}^{(p)} + \frac{\partial d}{\partial\bar{\delta}^{(p-1)}}\dot{\bar{\delta}}^{(p-1)} + \frac{\partial d}{\partial\bar{\delta}^{(p)}}\dot{\bar{\delta}}^{(p)} \approx \frac{\partial d}{\partial\lambda}\dot{\lambda} \tag{22}$$

The derivative $\partial d/\partial\lambda$ is readily obtained by differentiating Eq. (16) with respect to the equivalent separation norm λ. The time derivative $\dot{\lambda}$ is rewritten by the chain rule: $\dot{\lambda} = (\partial\lambda/\partial\Delta_k)\dot{\Delta}_k$. Inserting the definition of λ from Eq. (5), and carrying out the differentiation, one eventually arrives at Eq. (23).

$$\dot{d} = H^{(p)}\left[1 + \delta_{3k}\frac{\langle-\Delta_3\rangle}{\Delta_3}\right]\Delta_k\dot{\Delta}_k \tag{23}$$

Wherein $H^{(p)}$ is a scalar function of λ, as given by Eq. (24), and updates with the current line segment p.

$$H^{(p)} = \frac{\bar{\sigma}^{(p-1)}\bar{\delta}^{(p)} - \bar{\sigma}^{(p)}\bar{\delta}^{(p-1)}}{K^{(eq)}(\bar{\delta}^{(p)} - \bar{\delta}^{(p-1)})}\frac{1}{\lambda^3} \qquad \text{for } \bar{\delta}^{(p-1)} \le \lambda \le \bar{\delta}^{(p)} \tag{24}$$

Returning to Eq. (21) and substituting the expression for $\dot{d}$ therein, an explicit relation between $\dot{\tau}_i$ and $\dot{\Delta}_j$ is obtained. The constitutive tangent stiffness tensor is identified such that $\dot{\tau}_i = D_{ij}^{tan}\dot{\Delta}_j$, see Eq. (25). The situation dependent behaviour of the damage criterion in relation to the damage threshold value r, necessitates to split the computation of D_{ij}^{tan} into two cases. In case of loading $\lambda > r$ and in case of unloading/reloading $\lambda \le r$, the time derivative of the damage variable is $\dot{d} > 0$ and $\dot{d} = 0$, respectively. In the latter case, the second term in Eq. (21) vanish and the expression of D_{ij}^{tan} simplifies.

$$D_{ij}^{\tan} = \begin{cases} \delta_{ij}K^{(eq)}\left[1 - d\left(1 + \delta_{3j}\frac{\langle-\Delta_3\rangle}{\Delta_3}\right)\right] - K^{(eq)}\left[1 + \delta_{3i}\frac{\langle-\Delta_3\rangle}{\Delta_3}\right]\left[1 + \delta_{3j}\frac{\langle-\Delta_3\rangle}{\Delta_3}\right]H^{(p)}\Delta_i\Delta_j & \text{for } r < \lambda \le \bar{\delta}^{(n)} \text{ and } \bar{\delta}^{(p-1)} \le \lambda \le \bar{\delta}^{(p)} \\ \delta_{ij}K^{(eq)}\left[1 - d\left(1 + \delta_{3j}\frac{\langle-\Delta_3\rangle}{\Delta_3}\right)\right] & \text{for } r \ge \lambda \text{ or } \lambda > \bar{\delta}^{(n)} \end{cases} \tag{25}$$

3. Finite Element Implementation

The CZ model is implemented in an interface finite element. The interface element is formulated as an eight-noded bilinear isoparametric element of zero thickness in the undeformed state. An inherent and beneficial property of a multilinear CZ law, is the flexibility to attain any shape if the number of line segments is sufficiently high. However, the piecewise formulation and the discontinuous slopes add complexity to the numerical implementation, and request schemes to monitor the currently active line segment in the CZ law in order to update p in the CZ variables: $\bar{\delta}^{(p-1)}$, $\bar{\sigma}^{(p-1)}$, $\bar{\delta}^{(p)}$, and $\bar{\sigma}^{(p)}$.

To validate the implementation of the constitutive damage model, a FE model consisting of a single interface element is considered in Fig. 5. The lower surface of the interface element is fixed and the upper surface is given a set of prescribed displacements in the UX, UY, and UZ which directly corresponds to local separations Δ_1, Δ_3, and Δ_2, respectively. The resulting nodal stress-displacement curves should give an exact replica of the input CZ law for the constitutive damage model to be implemented correctly.

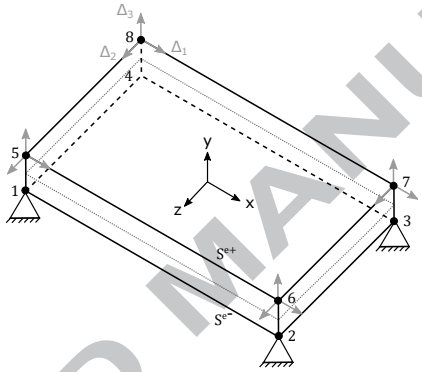

Figure 5: A FE model consisting of a single interface element for verification studies.

3.1. Pure Mode I Verification

Four different shapes of a 6-segmented multilinear CZ law is considered to demonstrate characteristics and limitations of the current FE implementation. The CZ laws under consideration is illustrated by the green curves in Fig. 6(a) through (d). Fig. 6(a) represents a typical monotonically softening CZ law. Fig. 6(b) represents a CZ law with a sudden drop in traction and with line segments of zero- and infinite slope. Fig. 6(c) represents a CZ law which hardens gradually after some amount of initial softening. Fig. 6(d) gives an example of a CZ law which violates the basic damage criterion in Eq. (14) when using a secant stiffness-based damage variable. The latter example is included to demonstrate a limitation of the present formulation.

The upper surface nodal degrees of freedom are varied such that $UX = UZ = 0.00$mm and UY is prescribed in the following sequence: The normal separation component is varied from $UY = 0.00$mm to $UY = 1.67$mm, then unloaded until $UY = 0.00$mm, and lastly reloaded from $UY = 0.00$mm until final failure at $UY = 6.00$mm. The light blue crosses represent converged solution outputs from the FE simulation. In cases Fig. 6(a)-(c) the present formulation works as intended, since the output of the FE simulation lies on top of the input CZ law. The linear unloading/reloading and damage threshold implementation also works properly, since the solution outputs follow a line of secant stiffness $K^{(eq)}(1-d)$ when unloading/reloading between $UY = 1.67\text{mm} \rightleftharpoons 0.00\text{mm}$.

The example in Fig. 6(d) violates the basic damage criterion in Eq. (14), as the secant stiffness $K^{(eq)}(1-d)$ does not decrease monotonically when passing through $\delta_3 = 1.00$mm. This implies that the stiffness-based damage variable would necessarily have to decrease. In this example, the simulation output fail to unload/reload along the path of secant stiffness.

Conclusively, the multilinear formulation works as intended for a wide range of shapes of the CZ law. Severe sawtooth-like shapes can cause complications between the numerical implementation and the damage criterion, however, these shapes are impractical for most real material systems.

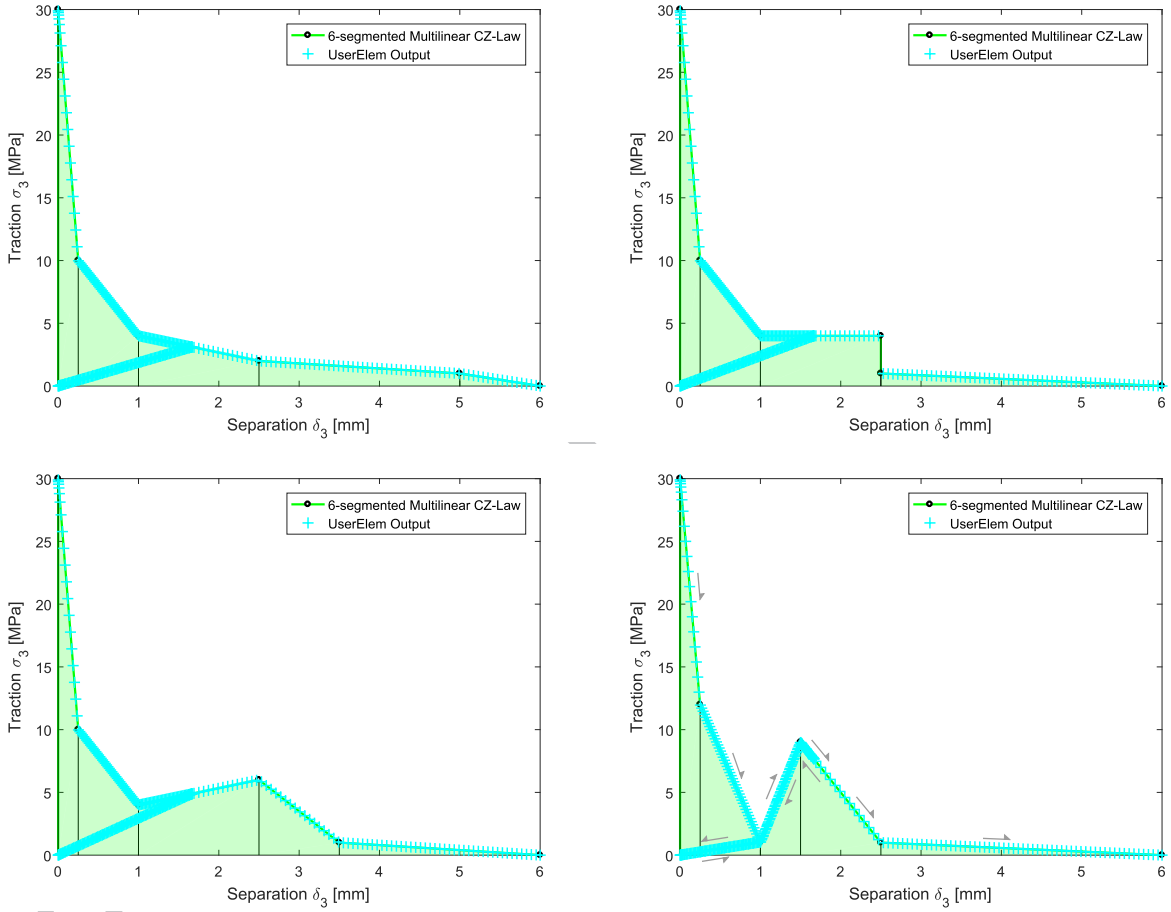

Figure 6: Pure mode I loading/unloading/reloading tests, for various shapes of a 6-segmented multilinear CZ law. Top-left: (a) Typical softening CZ law. Top-right: (b) CZ law of horizontal and vertical line segments. Bottom-left: (c) One line segment of positive slope after onset of damage. Bottom-right: (d) Sever zig-zagging in CZ law.

3.2. *Mixed-mode Verification*

Having demonstrated the constitutive damage formulation in loading/unloading/reloading sequences for an arbitrary multilinear CZ law under pure mode I crack opening, mixed-mode crack openings are now studied. For this purpose, the same FE model as shown in Fig. 5 is considered. Three verification tests are performed for three different mode-mixity ratios β. Depending on the value of β, the prescribed displacements UX, UY and UZ are set differently. The β value and prescribed displacements appear in Tab. 1 for the three tests. Values of $\beta = 1.0$ and $\beta = 0.0$ corresponds to pure mode s and pure mode I crack opening, respectively.

Recall that the equivalent one-dimensional CZ laws are defined according to the interpolation formulas in Eq. (7) and Eq. (13). The curve fitting exponents, ξ and η, are set to be equal $\xi = \eta = 1.40$ for these tests. The intended CZ laws are shown by solid curves in Fig. 7 and 8, and the light blue crosses represent converged outputs from the simulations. The FE simulations agree with the input CZ laws and therefore the implementation is concluded to be verified.

Mode-mixity ratio, β	UX	UY	UZ
0.00	0.00	8.00	0.00
0.41	3.90	5.70	0.00
1.00	5.00	0.00	0.00

Table 1: Prescribed displacements for three tests of different mode-mixity ratio.

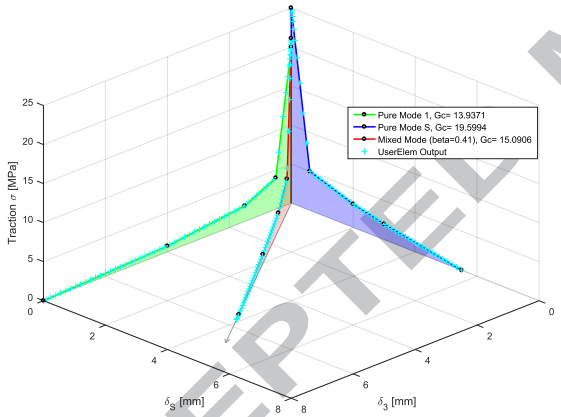

Figure 7: Green: Pure mode I. Blue: Pure mode S. Red: Mixed-mode $\beta = 0.41$.

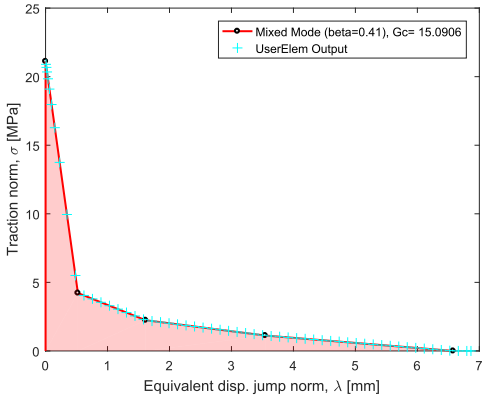

Figure 8: The mixed-mode verification test from Fig. 7 is shown in the plane of the λ-axis, for constant mode-mixity ratio $\beta = 0.41$.

4. An Application of the Multilinear CZ Law to Simulate Mode I Delamination with R-curve Effects

The proposed multilinear CZ law is applied to simulate quasi-static delamination in a real experiment using materials with R-curve effects. The experimental data are obtained from [25], to which the reader is referred to for further details. A brief explanation of the experiment is given here. The experiment is conducted on a laminated DCB specimen made of uni-directional glass fiber-epoxy using the vacuum assisted resin transfer molding process. The specimen length, width and thickness are 273.0mm, 24.8mm and 9.0mm, respectively, and an initial crack of length 66.0mm is introduced during the manufacturing of the specimen by a 0.13μm thick PTFE film. Elastic material properties are given according to Tab. 12. The DCB specimen is subjected to equal and opposite bending moments at the DCB arm ends, as illustrated in Fig. 9, which results in pure mode I crack opening. The applied moment and the angle of rotation of the DCB arms are monitored during the experiment and are shown by the black curve in Fig. 10.

A FE model of the DCB specimen similar to that of the experiment is constructed in ANSYS Mechanical APDL, which is shown in Fig. 11. The specimen bulk material is modelled using eight-noded linear solid elements, with an enhanced assumed strain formulation to avoid shear locking. A predefined crack plane is introduced along the interface of the upper and lower DCB arms at $Y = 0$. The interface is modelled with a user-defined cohesive interface element. The cohesive interface element is an eight-noded linear isoparametric element whose kinematic model is described in Sec. 2.1 and relies on the constitutive damage model and corresponding multilinear CZ law as proposed in the present work. The mesh of the DCB model is divided into regions of fine and coarse discretization. A refined solid element mesh with element length/width/height of 0.25mm / 0.50mm / 2.25mm is used in the region of potential crack growth, while a coarse mesh is used in the remaining. The FE model is subjected to prescribed rotations using multi-point-constraint techniques to mimic the loading experienced in the real experiment and to have a displacement controlled FE model. The nonlinear problem is solved incrementally using a Newton-Raphson solver with default settings in ANSYS.

The multilinear CZ law may possess a high number of degrees of freedom to enable constitutive modelling of complex and multi-scale fracture processes. A key challenge in applying the multilinear CZ law, and other advanced CZ laws in general, is model calibration. The model calibration can be achieved in several different ways, e.g. [13, 16, 18, 19, 26]. In this work, a recently developed methodology [27], which relies on inverse parameter identification, has been applied to calibrate the CZ variables of the CZ laws under consideration. The methodology in [27] is an inverse approach, which identifies CZ laws by iteratively varying CZ variables using a gradient-based optimization scheme to minimize the error in structural response between a physical experiment and a parametric finite element model. The reader is referred to [27] for a comprehensive description of the methodology. Essential settings of the methodology are the choice of structural responses to include in the error function to be minimized, and the number of linear segments to include in the multilinear traction-separation relation. However, it is proved in [27] that the inverse parameter identification procedure is robust and provides shape-consistent CZ laws, which converge to a particular CZ law as the number of line segments is increased. In the present study, the focus is to demonstrate an application of the proposed CZM. The predictive capability of R-curve effects are compared using bi-, trilinear CZ laws and a 15-segmented multilinear CZ law. All the CZ laws are obtained with the inverse parameter identification procedure in [27], as the traction-separation relations that reproduce the global response curve in Fig. 10 at best. The CZ laws are shown in Fig. 13. Note the CZ laws are split into two figures of different scales for illustration purposes. The simulated response using the 15-segmented multilinear CZ law is shown by the blue curve in Fig. 10. The response agrees well with the experimental data and accurately simulates R-curve effects. The need for a multilinear CZ law is emphasized in Fig. 10, by comparison of the structural response to those obtained using a bi- and a trilinear CZ law. The bilinear CZ law does not have the ability to model R-curve behaviour. The trilinear CZ law can represent the R-curve behaviour to some extent, but requires a low onset traction to obtain a reasonable agreement with the experimental response, which compromises the quality of crack initiation predictions. Additionally, the trilinear CZ law predicts non-physical kinks in the structural response, and represents the slopes of the structural response curves poorly. The multilinear CZ law in Fig. 13 substantiate that the cohesive tractions near the crack tip and the bridging tractions in the wake of the crack tip are far more complex than the simplified linear-smearing done with the conventional bi- and trilinear CZ laws.

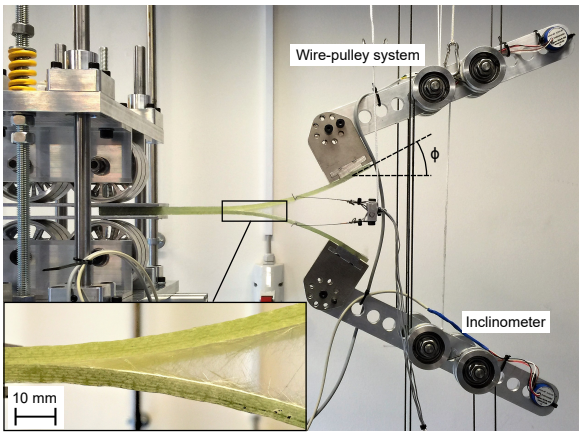

Figure 9: Photography of the DCB specimen during the experiment. The load is applied to the DCB arms through rigid metal beams and a wire-pully system connected to a tensile testing machine. The angle of rotation is measured using inclinometers attatched to the metal beams.

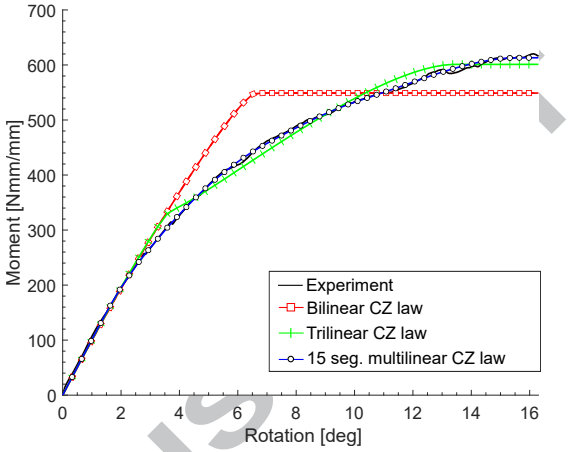

Figure 10: Structural response in terms of the angle of rotation and applied moment for the upper DCB arm. The red curve shows the experimental data, while the blue curve shows the output from the FE model using a CZ law as shown in Fig. 13.

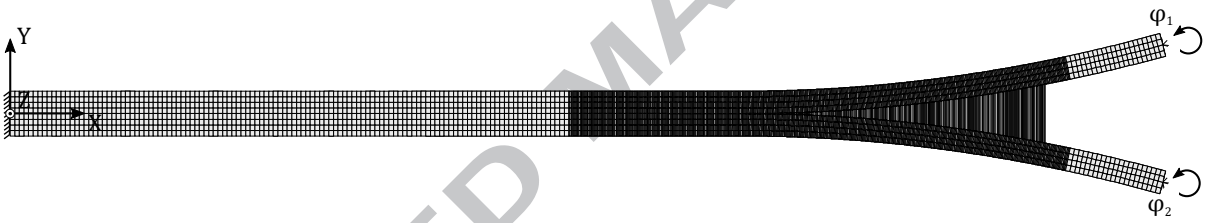

Figure 11: FE model of DCB specimen. Equal and opposite rotations are applied at each DCB arm $\varphi_2 = -\varphi_1$, resulting in pure mode I crack opening.

Elastic material properties								
E_{xx}	E_{yy}	E_{zz}	ν_{xy}	ν_{yz}	ν_{xz}	G_{xy}	G_{yz}	G_{xz}
$21.4GPa$	$10GPa$	$10GPa$	0.30	0.07	0.30	$4GPa$	$2.5GPa$	$4.0GPa$

Figure 12: Table of material properties for the experiment and FE model.

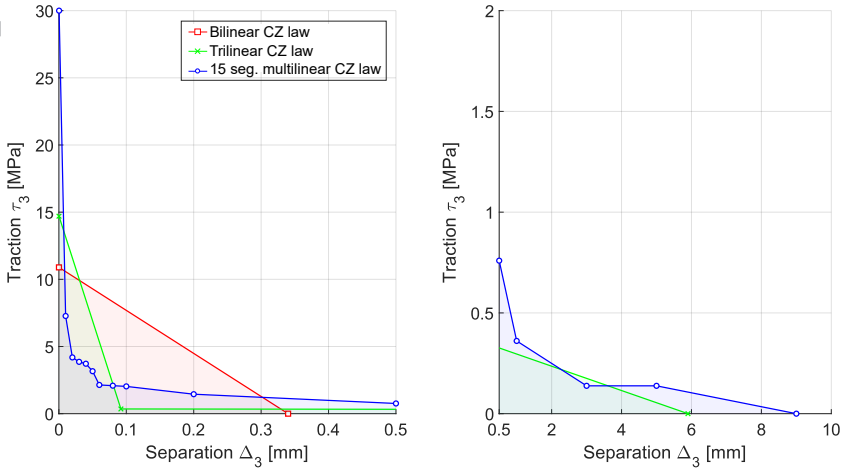

Figure 13: Bi-, tri- and multilinear CZ laws used in the FE model to simulate the experiment. The CZ laws are split in two graphs of different scales for illustration purposes.

5. Conclusion

The work develops a constitutive damage model in a cohesive interface element for implicit FEA of quasi-static delamination in material systems with large-scale fiber bridging. The paper proposes a mixed-mode multilinear CZ law to add degrees of freedom to the shape of the CZ law, and thereby improve the quality of existing CZ models in modelling complex and multi-scale fracture processes. A set of interpolation formulas for determining equivalent one-dimensional CZ variables of a general mixed-mode multilinear CZ law is derived. The interpolation formulas are based on quadratic stress interaction and are energy consistent with the modified BK-criterion. Additionally, a constitutive tangent stiffness tensor is derived, and the complete constitutive damage model is implemented and verified through user-programmable features in ANSYS Mechanical APDL. The novel formulation enables simulating delamination in material systems exhibiting severe R-curve behaviour. The quality is demonstrated by simulating an experiment of quasi-static crack initiation and growth in glass fiber-epoxy laminates. The impact of the work is emphasized by comparing simulated responses obtained using the present formulation and conventional formulations. The simulated response using the multilinear CZ law shows excellent agreement with experimental measurements of the delamination process when large-scale bridging are present. The generality of the proposed CZM and interface finite element formulation makes the multilinear CZ law compatible with recent developments in CZM such as the method for evaluation of mode-decomposed energy release rates in three-dimensional delamination problems with large fracture process zones [28] and the concept of growth driving directions [21]. In this context the quality of the multilinear CZ law to model R-curve behaviour maybe exploited in future works.

References

[1] G. I. Barenblatt, The mathematical theory of equilibrium cracks in brittle fracture, Journal of Advance Applied Mechanics 7 (1962) 55–129.

[2] D. S. Dugdale, Yielding of steel sheets containing slits, Journal of the Mechanics and Physics of Solids 8 (1960) 100–104.

[3] A. Hillerborg, M. Modeer, P. E. Petersson, Analysing of crack formation and crack growth in concrete by means of fracture mechanics and finite elements, Cement and Concrete Reseach 6 (1976) 773–782.

[4] A. Needleman, A continuum model for void nucleation by inclusion debonding, Journal of Applied Mechanics 54 ((3)) (1987) 525–531.

[5] P. P. Camanho, C. G. Davila, M. F. De Moura, Numerical simulation of mixed-mode progressive delamination, Composite Materials 37, No. 16/2003.

[6] A. Turon, P. Camanho, J. Costa, J. Renart, Accurate simulation of delamination growth under mixed-mode loading using cohesive elements: Definition of interlaminar strength and elastc stiffness, Composites Structures (2010) 1857–1864.

[7] A. L. Hansen, E. Lund, B. F. Sørensen, Simulation of crack growth and r-curve behavior using cohesive zone modeling, *Unpublished* (2009).

[8] B. L. V. Bak, E. Lindgaard, E. Lund, Analysis of the integration of cohesive elements in regard to utilization of coarse mesh in laminated composite materials, International Journal for Numerical Methods in Engineering 99(8) (2014) 566–586. doi:10.1002/nme.4688.

[9] V. Tvergaard, J. W. Hutchinson, The relation between crack growth resistance and fracture process parameter in elastic-plastic solids, Journal of the Mechanics and Physics of Solids 40 (6) (1992) 1377–1397.

[10] V. K. Goyal-Singhal, E. R. Johnson, C. G. Davila, Irreversible consititutive law for modeling the delamination process using interfacial surface discontinuities, Composite Structures 65 ((3)) (2004) 289–305.

[11] A. Turon, J. Costa, P. Camanho, C. Davila, Simulation of delamination in composites under high-cycle fatigue, Composites Part A 38 (2007) 2270–2282.

[12] G. Alfano, On the influence of the shape of the interface law on the application of cohesive-zone models., Composites Science and Technology 66 (6) (2006) 723–730.

[13] B. F. Sørensen, T. K. Jacobsen, Large-scale bridging in composites: R-curve and bridging laws, Composites Part A 29A (1998) 1443–1451.

[14] E. Farmand-Ashtiani, J. Cugnoni, J. Botsis, Specimen thickness dependence of large scale fiber bridging in mode i interlaminar fracture of carbon epoxt composites, International Journal of Solids and Structures 55 (2014) 58–65.

[15] L. P. Canal, M. Alfano, J. Botsis, A multi-scale based cohesive zone model for the analysis of thickness scaling effects in fiber bridging, Composites Science and Technology 139 (2017) 90–98.

[16] L. Sorensen, J. Botsis, T. Gmür, L. Humbert, Bridging tractions in mode i delamination: Measurements and simulations, Composites Science and Technology 68 (2008) 2350–2358.

[17] V. Tamuzs, S. Tarasovs, U. Vilks, Progressive delamination and fiber bridging modelling in double cantilever beam composite specimens, Engineering fracture mechanics 68 (2001) 513–525.

[18] M. Heidari-Rarani, M. M. Shokrieh, P. P. Camanho, Finite element modelling of mode i delamination growth in laminated dcb specimens with r-curve effects, Composites: Part B 45 (2012) 7.

[19] A. Airoldi, C. Davila, Identification of material parameters for modelling delamination in the presence of fibre bridging, Composite Structures 94 (2012) 3240–3249.

[20] E. Lindgaard, B. Bak, J. Glud, J. Sjølund, E. Christensen, A user programmed cohesive zone finite element for ansys mechanical, Engineering Fracture Mechanics 180 (2017) 229–239.

[21] L. Carreras, B. Bak, A. Turon, J. Renart, E. Lindgaard, Point-wise evaluation of the growth driving direction for arbitrarily shaped delamination fronts using cohesive elements, European Journal of Mechanics / A Solids 72 (2018) 464–482.

[22] A. Turon, P. Camanho, J. Costa, C. Davila, A damage model for the simulation of delamination in advanced composite under variable-mode loading, Mechanics of Materials 38 (2006) 1072–1089.
[23] M. L. Benezeggagh, M. Kenane, Measurement of mixed-mode delamination fracture toughness of unidirectional glass/epoxy composites with mixed mode bending apparatus, Composites Science and Technology 56 (4) (1995) 439–449.
[24] J. R. Rice, A path independent integral and the approximate analysis of strain concentration by notches and cracks, Journal of Applied Mechanics 35 (1968) 379–386.
[25] E. Lindgaard, B. Bak, Experimental characterization of delamination of off-axis gfrp laminates during mode i loading, Submitted to Composite Structures *(under review)*.
[26] B. Sørensen, T. Jacobsen, Determination of cohesive laws by the j integral approach, Engineering fracture mechanics 70 (2003) 1841–1858.
[27] S. Jensen, M. Martos, E. Lindgaard, B. Bak, Inverse parameter identification of n-segmented multilinear cohesive laws using parametric finite element modeling, Submitted to Composite Structures (*under review*).
[28] L. Carreras, E. Lindgaard, J. Renart, B. Bak, A. Turon, An evaluation of mode-decomposed energy release rates for arbitrarily shaped delamination fronts using cohesive elements, Computer methods in applied mechanics and engineering *In press (2018)*.